

Zaid H. Al-Sawaff^{1,2}, Serap Senturk Dalgic³, Zaheda A. Najim⁴, Shatha S. Othman⁵,
Fatma Kandemirli⁶

A Comparative Density Functional Theory Study of BMSF-BENZ Chemisorption on Zn₁₂O₁₂, Al₁₂P₁₂ Nanocages

¹Material Science & Engineering Dept., Faculty of Engineering and Architecture, Kastamonu University, Turkey,
zaidalsawaff@ntu.edu.iq

²Medical Instrumentation Technology, Technical Engineering College, Northern Technical University, Mosul, Iraq

³Department of Physics, Faculty of Science, Trakya University, 22030, Edirne, Turkey

⁴College of Education for Pure Science, Mosul University, Mosul, IRAQ

⁵Medical Instrumentation Technology, Technical Engineering College, Northern Technical University, Mosul, Iraq

⁶Biomedical Engineering Department, Faculty of Engineering & Architecture, Kastamonu University,
Kastamonu, Turkey

The present study aims to investigate the potential and capability of Zinc-Oxide nanocage and aluminum phosphide nanocage to detect and adsorb ((4-Bromo-7-methoxy-1-(2-methoxyethyl)-5-[[3-(methylsulfonyl)phenyl]methyl]-2-[4-(propane-2-yl)phenyl]-1H-1,3-benzothiazole) molecular. For this purpose, we selected seven stable locations for BMSF-BENZ to be adsorbed on the surface of these nanocages. All considered configurations are optimized using DFT theory at the 6-31G** basis set and B3LYP level of theory. Then from optimized structures, the Quantum theory of atom in the molecule (QTAIM), Reduced density gradient (RDG) Analysis, and Molecular Orbital Analysis (MO) were performed.

The results showed that the reaction of BMSF-BENZ with the nanocages was highly exothermic, indicating the high chemical adsorption of the new complexes. The adsorption energies on the ZnO nanocage were higher than those of AIP for all the investigated active atoms in the drug complex, where the adsorption energies were (-28.20, -37.86, -27.36, -23.59, -30.30, -42.55, and -32.49) Kcal/mol, and (-17.03, -28.30, -15.45, -16.70, -18.22, -18.35, and -18.64) Kcal/mol for ZnO and Al-P nanocages respectively.

Topology analyses such as QTAIM and NCI/RDG indicate that the interactions between the BMSF-BENZ drug and the surface of the ZnO nanocage are more substantial than those of the AIP nanocage. The results of the obtained charge, the total density of states (TDOS), and molecular orbital-boundary analysis confirm a characteristic orbital hybridization upon adsorption of BMSF-BENZ, indicating the potential application of AIP as a biochemical adsorbent for BMSF-BENZ. Nevertheless, ZnO nanocage could be a candidate for drug delivery applications.

Keywords: drug adsorption; BMSF-BENZ; nanocages; drug delivery system; density functional theory; thermodynamic properties.

Received 8 December 2021; Accepted 31 January 2022.

Introduction

Osteoporosis [1] is one of the most common diseases among the elderly, especially in women. This disease causes a decrease in bone mass and a deterioration of the delicate structure of bone tissue, thus an increase in the

rate of fracture [2].

Currently, most drugs used to treat osteoporosis prevent bone resorption and further loss of bone mass. Still, since most people with this disease have already lost a significant amount of their bone mass, there is an urgent need to develop new drugs that improve or stimulate the growth of their bone mass [3]. The best drugs used in the

treatment of osteoporosis depend on the elevated levels of the hormone (PTH), which stimulates the production of bone mass and increases bone mass through the (CaSR) inhibitor. Still, the main problem in these drugs is focused on the time required to absorb it along with the time needed to get rid of it, i.e., a sharp difference between them should be obtained (short Tmax) [4]. Therefore, in this research, one of the best-approved drugs in the treatment of osteoporosis-related with the BMSF-BENZ family is has been studied (Fig. 1-A), with its chemical structure (4-Bromo-7-methoxy-1-(2-methoxyethyl)-5-[[3-(methylsulfonyl) phenyl]methyl]-2-[4-(propane-2-yl)phenyl]-1H-1,3-benzothiazole), which is characterized by having appropriate properties concerning the peak of hormone release (PTH) and (CaSR) inhibitor based on the practical studies of the physical and chemical properties of this drug [4].

In recent years, nanocages have been studied extensively by studying their effects on the host compound or by examining their chemical and physical properties, such as adsorption properties, sensitivity towards some drugs, hydrophobic properties [5-8]. Significant efforts have been made by scientists and researchers over the past years towards the manufacture of tubular and spherical fullerenes from inorganic (non-carbon) materials and the use of various materials such as zinc oxide (ZnO), aluminum phosphide (AlP), and other active chemical compounds in addition to the use of carbon nanotubes and fullerenes (C₆₀) in most modern and advanced devices. Studies have shown that (XY)_n groups, X₁₂Y₁₂ (X = Al, B, Ga, and Y = As, N, P), are the most stable "the magical groups"[9]. Also, the possibility of exploiting these distinct properties improves the shape of the final drug compound in terms of the speed of drug delivery or the amount of drug that is delivered to the target, whether the nanoparticle used is of the type of nanocages or nanotubes [10-13].

The nanocages used in this research depended on the unique and appropriate properties to deliver drugs faster than others. The first nanoparticle used is the zinc oxide nanocage (Zn₁₂O₁₂) (Fig. 1-B) which is considered a material that shows suitable thermal properties and contains semiconductor properties in addition to piezoelectric properties [14]. Typically, these nanocages are manufactured using vapor-phase thermal sublimation techniques and under specific growth conditions [15-18].

These nanocages have proven to be probably one of the wealthiest groups of nano-structures among all other

materials, as they can be used in biosensors and drug delivery systems in addition to their applications in biomedical sciences because they are considered a biologically safe material [19].

The second nanoparticle used in this article is the aluminum phosphide (AlP) nanocage [20]. The nanostructure of this compound, especially (Al₁₂P₁₂) compound (Fig. 1-C), has received wide attention from scientists due to its low electron levels, large energy gap, as well as exceptional chemical-physical properties as it enhances the minerals adsorption on its surface and exhibits multiple properties like the stimulatory and sorption [21, 22].

Several literature studies showed that using these types of nanocages on a group of drugs has a promising future in drug delivery and improving adsorption efficiency on their surfaces [23, 24].

As mentioned earlier, several literature reviews have discussed using these specific types of nanocages due to their importance and unique properties. This section will try to review the most critical and recent literature on this topic.

In 2018, Baei Mohammad T. proposed a DFT study on C₂₀ and its AlnPnC_{20-2n} hetero-fullerene derivatives. The vibrational frequency calculations show that other species are valid minima exclusive of Al₆P₆C₈ and Al₁₀P₈C₂. They proved that in both gas phase and polar solvent, the Al₁₁P₁C₁₈ structure is expected to be stabilized to a greater extent than the other species, which the thermodynamic and kinetic data have confirmed [25].

Lv et al. in 2020 produced a novel "turn-on" sensing platform for Cu²⁺ detection that was established using ZnO-Co₃O₄ NCs nanocage where its strong binding ability toward Cu²⁺ enabled the ZnO-Co₃O₄ NCs/Cys system to be used for detection of Cu²⁺. The sensor has an excellent linear range of 2 to 100 nM with a detection limit of 1.08 nM. Due to the high sensitivity and selectivity, the proposed assay was also successfully applied for quantitative measurement of Cu²⁺ in serum without pretreatment [26].

Emphasis has been placed on using ZnO and AlP nanocages due to their exceptionally high adsorption capacity, large HOMO-LUMO gap, low electron attraction, and other outstanding physical and chemical properties [27-31].

Recently, the adsorption of BMSF-BENZ on a group of nanocages and nanotubes was studied [32], but ZnO and AlP nanocages were not included, so based on the authors'

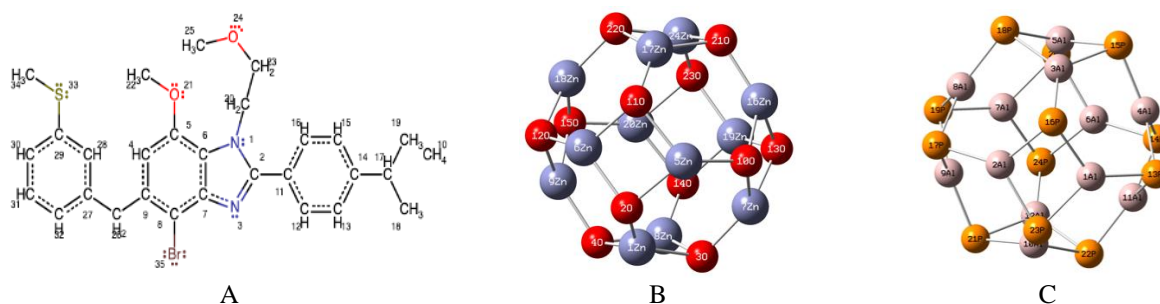


Fig. 1. Chemical structure of BMSF-BENZ and the optimized structure of Zn₁₂O₁₂ nanocage before combining the together A. BMSF-BENZ, B. Optimized structures of Zn₁₂O₁₂ nanocage, and C. Optimized structures of Al₁₂P₁₂ nanocage.

knowledge, the adsorption of BMSF-BENZ was not studied on these nanocages.

In this paper, a DFT comparative study is proposed to investigate the adsorption behavior of the BMSF-BENZ drug complex on the surface of two selected nanocages, Zinc-Oxide ZnO nanocage, and aluminum-phosphide AIP nanocage. This study included some chemical properties, electronic analysis of the compounds, QTAIM analysis, and NCI / RDG analysis in order to reach the best choice among the selected nanocages, to be considered as a means for the most appropriate drug delivery vehicle.

I. Computational methods

This section discusses mathematical calculations using the DFT theory about the adsorption of the BMSF-BENZ molecule on AIP and ZnO fullerene-like cage surfaces. Initially, the relaxed structure of BMSF-BENZ systems/adsorbents, values of adsorption energy, the total density of states (TDOS), and charge transfer were calculated and analyzed. All operations were performed using the Gaussian09 program package [33] at the B3LYP/6-31G(d,p) level of DFT. The geometry optimizations were performed without any constraints under default parameters for optimization in Gaussian 09. The maximum force and RMS forces are 3×10^{-4} and 4.5×10^{-4} (Hartree's/Bohr and Hartree's/Radian), whereas maximum displacement and RMS displacement are 1.8×10^{-3} and 1.2×10^{-3} .

Also, we analyzed the vibrational frequencies of all the new complexes compared to the original compounds to verify the actual global minima for the expected nanoparticle. The adsorption energy, energy gap change, charge transfer analysis, dipole moment, and recovery time are also investigated to prophesy the interaction of drug molecules with nanocages.

In order to obtain the electrical properties of complexes, the energies of the highest occupied molecular orbital E_{HOMO} and the lowest occupied molecular orbital E_{LUMO} are calculated. Also, some physicochemical parameters based on E_{HOMO} and E_{LUMO} energies, such as electronegativity (χ), Fermi energy level (E_f), energy gap (E_g), are calculated using the following equations: [34-38]:

$$\chi = -\frac{1}{2} (E_{HOMO} + E_{LUMO}) \quad (1)$$

$$E_f = E_{HOMO} + \left(\frac{E_{LUMO} - E_{HOMO}}{2} \right) = -\chi \quad (2)$$

$$E_g = E_{LUMO} - E_{HOMO} \quad (3)$$

The adsorption energies of the BMSF-BENZ drug on the surfaces of the nanocages are obtained by [37]:

$$E_{ads} = E_{complex} - (E_{nanocage} + E_{drug}) \quad (4)$$

$E_{Complex}$, $E_{Nanocage}$, and E_{Drug} indicate the energy of the complex composed of nanocages/the drug and energies isolated from nanocage and drug, respectively. E_{ads} energy is determined from the summation of the interaction energy E_{int} and deformation energies E_{def} of the drug E_{def}

and the nanocages $E_{def-nanocage}$ through the adsorption process [37].

$$E_{int} = E_{complex} - (E_{nanocage \text{ in complex}} + E_{drug \text{ in complex}}) \quad (5)$$

$$E_{def} = (E_{drug \text{ in complex}} - E_{drug}) + (E_{nanocage \text{ in complex}} - E_{nanocage}) \quad (6)$$

$E_{nanocage}$ and E_{drug} in the complex are the energies of nanocage and drug with their geometries in the complex, respectively.

On the other hand, thermodynamic parameters such as the change in Gibbs free energy (ΔG), entropy (ΔS), and enthalpy (ΔH) are investigated to analyze the structural stability using the following equations [39]:

$$\Delta G = G_{complex} - G_{nanocage} - G_{drug} \quad (7)$$

$$\Delta H = H_{complex} - H_{nanocage} - H_{drug} \quad (8)$$

$$\Delta S = \frac{\Delta H - \Delta G}{T} \quad (9)$$

$G_{complex}$ and $H_{complex}$ are the Gibbs free energy, and the enthalpy of BMSF-BENZ adsorbed upon nanocages. G_{nano} and H_{nano} are the Gibbs free energy and enthalpy of the nanocages, G_{drug} and H_{drug} are the Gibbs free energy and enthalpy of the drug, respectively. T is the room temperature 298.15 K.

The nature of interactions between BMSF-BENZ and the nanocages has been determined by topology analysis of quantum theory of atoms in molecules (QTAIM) of Bader's [40], which is implemented in the MULTIWFN program [40]. The non-covalent interaction index (NCI) analysis was obtained through Multiwfn 3.7 program by the reduced density gradient (RDG) of quantum mechanical density of the electron. The RDG scatter plots versus the second largest eigenvalue of the Hessian matrix of electron density are created by Multiwfn 3.7 program [41]. Colored maps of scatter points of RDG are drawn by Gnuplot 5.2 program [42], while NCI isosurfaces were drawn by visual molecular dynamics (VMD) package [43].

The molecular orbital (MO) analysis has been evaluated by the total density of states (TDOS) using the Gauss Sum program [44]. Recovery time is calculated to understand the desorption processes of the drug molecule from the nanocage's surface when the adsorbents are in the gas phase.

II. Results and discussion

2.1. The structure of the relaxed systems

The optimized geometries of the investigated nanocages show that they contain both four- and six-sided rings. This is the same as what has been reported in other research [45], so we will not detail the information in this paragraph. It is worth noting that all the nanocage rings, whether they are quadrilateral or hexagonal, are not entirely flat or symmetrical.

In the ZnO nanocage, the dihedral angle in the quadrilateral is 7.29°, and the dihedral angle in the hexagonal ring is -14.88°. On the other hand, the measure of the dihedral angle was 26.83°, and the hexagonal angle was -45.51° for the cage of AIP.

Fig. 2 shows the different rings of the investigated nanocages where A refers to the four-sided ring, and B refers to the six-sided ring.

Bond length between the atoms differed depending on the nanocage, as shown in Table 1.

Through interaction with BMSF-BENZ, many notable changes in the geometric parameters of the investigated nanocages are recognized. The interaction between BMSF-BENZ and these nanocages is explained in expressions of binding energy and changes in the geometric parameters.

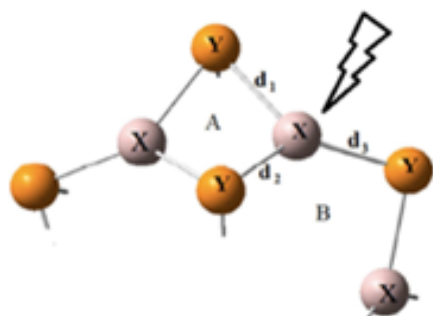


Fig. 2. The relaxed structure for $X_{12}Y_{12}$ ($X = \text{Zn}$ or Al , $Y = \text{O}$ or P).

The important geometric parameters with their binding energies are given in Table 2. Binding energies of BMSF-BENZ with ZnO through (Br, N_8 , N_9 , N_{58} , O_{35} , O_{42} , and S) atoms are (-28.20, -37.86, -27.36, -23.59, -30.30, -42.55, -32.49) Kcal/mol respectively, while for

AIP nanocage the energy values were (-17.03, -28.30, -15.45, -16.70, -18.22, -18.35, -18.64) Kcal/mol for the same active atoms in drug molecule.

Moreover, the binding distance of BMSF-BENZ with the nanocages was equal to 2.4 Å before the adsorption. Nevertheless, the binding distances are different after adsorption. High binding energies refer to the chemisorption of BMSF-BENZ on these nanocages. The highest binding energy of BMSF-BENZ has been recognized on ZnO nanocage, and it can be associated with the higher charge density on Zn than Al.

The nanocages react with the nitrogen atom (N_8) and Oxygen atom (O_{42}) with ZnO and AIP nanocages, respectively, in the drug molecule, as shown in Fig 3. Where the highest binding energy was obtained between the investigated nanocages with the drug molecule (-37.86) and (-28.30) Kcal/mol for (ZnO and AIP) nanocages, respectively, because the nitrogen atom used does not bind with any active atom or molecule that could affect the interaction between it and the nanocage.

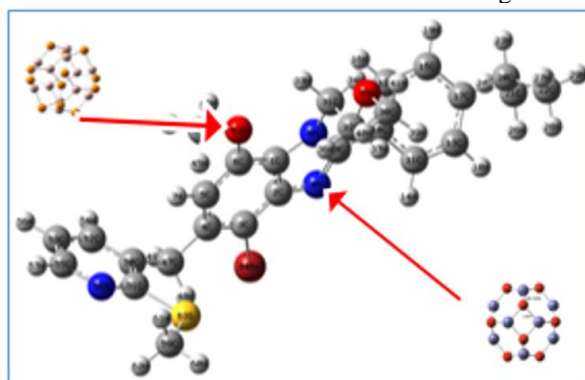


Fig. 3. Optimized structure of BMSF-BENZ compound with ZnO, and AIP nanocages combined in N_8 , O_{42} atoms respectively.

Table 1.

Bond angles, Dihedral angles, and Bond length before adsorption in ZnO and AIP nanocages.

	ZnO		AIP	
	Bond angles (degrees)	Bond length (Å)	Bond angles (degrees)	Bond length (Å)
X-Y-X (4)	87.06	1.93	74.73	2.34
Y-X-Y (4)	91.81	1.94	98.87	2.34
X-Y-X (6)	112.52	1.85	99.28	2.29
Y-X-Y (6)	126.29	1.93	130.10	2.34
	Dihedral angles (degrees)		Dihedral angles (degrees)	
X-Y-X-Y(4)	-14.88	-	-45.51	-
Y-X-Y-X(6)	7.29	-	26.83	-

Table2.

The new complexes of BMSF-BENZ/nanocage, the bond distance of the new complexes in Å, recovery time (sec), and the adsorption energy (Kcal/mol). The numbering is shown in Fig.2.

Structure	Distance (Å) After adsorption	Recovery time	Eads	Structure	Distance (Å) After adsorption	Recovery time	Eads
$Zn_{12}O_{12}$				$Al_{12}P_{12}$			
Br	2.51	1.51×10^4	-28.20	Br	2.61	9.98×10^{-5}	-17.03
N_8	2.05	1.80×10^{11}	-37.86	N_8	2.06	1.79×10^4	-28.30
N_9	2.91	3.68×10^3	-27.36	N_9	2.93	6.94×10^{-6}	-15.45
N_{58}	2.10	63.5	-23.59	N_{58}	2.10	5.67×10^{-5}	-16.70
O_{35}	2.10	5.23×10^5	-30.30	O_{35}	2.00	7.37×10^{-4}	-18.22
O_{42}	2.13	4.91×10^{14}	-42.55	O_{42}	2.00	9.24×10^{-4}	-18.35
S	2.55	2.08×10^7	-32.49	S	2.65	1.51×10^{-3}	-18.64

BMSF-BENZ adsorption causes significant changes in the nanocages geometry, and this effect decreases with distance from the adsorption position. Chemical adsorption, as indicated by the binding energies, produces a difference in the aluminum-zinc hybridization from nanocages from Sp_2 to Sp_3 , resulting in the aluminum and zinc atoms protruding out of the cage frame. The structural parameters are analyzed and presented in Table 1.

At first, the bond length between the nanocage and the BMSF-BENZ molecule is 2.4 Å, but after adsorption, the bond length became different, Table 2 shows the changes in bond length after adsorption, the binding energy and other recovery time needed for all new complexes.

As an example of the changes that occurred in the nanocage after the adsorption process, we took one of the new compounds (BMSF-BENZ- $N_8/Zn_{12}O_{12}$) and (BMSF-BENZ- $O_{42}/Al_{12}P_{12}$), where the most significant value of energy obtained was for it, and therefore the change was apparent on the features of the nanocage. Initially, the bond length between the nanocage and the drug compound became 2.08, 2.06 Å for the zinc oxide nanocage (ZnO) and the Aluminum phosphide nanocage (AlP), respectively. The angles between nano atoms changed to values that showed the zinc atom and the aluminum atom interacting with the active nitrogen atom in the drug compound forward as a result of the interaction.

In the zinc atom, the angle became in the quaternary ring 91.35 Å and the hexagonal ring 126.27 Å, while the aluminum atom in the other nanocage became 2.34 Å for the quaternary ring and 2.34 Å for the hexagonal ring.

The distance between the nanocage atoms was also affected by the nature of the adsorption by the drug compound, where the bond length (AlP) was equal to 2.34 Å in the tetragonal ring and 2.29, 2.34 Å for (AlP, PAI) respectively in the hexagonal ring. However, After the adsorption process, it became as follows (2.35, 2.33, 2.33, 2.35) Å for (AlP, PAI, AlP, PAI) respectively for the quaternary ring, and (2.30, 2.35, 2.27, 2.41, 2.36, 2.30) Å for (AlP, PAI, AlP, PAI, AlP, PAI) respectively.

A set of changes also occurred for the zinc atom after it was adsorbed by the active nitrogen atom in the drug compound, where the length of the distance between the zinc atom and its neighboring oxygen atoms was (1.98, 1.93, 1.90, 1.95) Å for the quaternary ring, and (1.85, 1.93, 1.84, 1.98, 1.88, 1.91) Å for the hexagonal ring. As for the angles, they also had their share of change, as shown in Table 2. This indicates a strong interaction between these nanocages and the BMSF-BENZ compound, which makes them promising compounds for use as a drug delivery vehicle.

The recovery time (adsorption time) is one of the critical parameters utilized for both gas sensors and drug delivery systems, which prognosticates the amount of time expected for drug adsorption from the adsorbent, as it is highly linked to the adsorption energy, and it is known that a high adsorption reaction needs a high adsorption time and vice versa. The recovery time can be calculated by the equation [46]:

$$\tau = \frac{1}{\nu} \text{Exp}\left(\frac{-E_{ads}}{kT}\right). \quad (10)$$

Where T, k, and ν are the temperature, Boltzmann's

constant and the attempted frequency, respectively. $k = 2 \times 10^{-3}$ kcal/mol K.

A different recovery time was obtained for all the new compounds after adsorption of BMSF-BENZ onto the nanocages (Table 2). Recovery time is calculated in vacuum UV-light conditions with frequencies of 3×10^{16} Sec⁻¹ at room temperature.

The results showed in Table 2 that the most significant value of the adsorption energy was at the bonding of the nanocage (ZnO) with the drug compound at the oxygen atom (O_{42}) with a value of (-42.55) Kcal/mol, and at the nitrogen atom (N_8) with the nanocage (AlP) with a value of (-28.30) Kcal/mol, which makes them suitable compounds to be used as drug delivery vehicles, However, the recovery time values were relatively high.

2.2. QTAIM Analysis

The characterization and classifications of intermolecular interactions have been of enormous interest in the last five decades. In DFT-based calculations, the electron density topological properties can be investigated by the powerful method of Bader's theory of atoms in molecules (AIM) to analyze the interactions nature. As reported earlier, the sign of the Laplacian of electron density of $\nabla^2 \rho(r)$ at BCP indicates the nature of bonding such as closed-shell (ionic, non-covalent, van der Waals type) and shared-shell (covalent) interactions.

Referring to Bader's quantum theory of atoms in molecules (QTAIM), closed-shell interactions should have a low electron density $\rho(r)$ with a positive value of $\nabla^2 \rho(r)$, whereas a high value of $\rho(r)$ with negative $\nabla^2 \rho(r)$, indicate the shared type (covalent) bonding. $\nabla^2 \rho(r)$ are positive for ionic and typical inter-molecular bonds.

The criterion proposed by Cremer and Kraka [47] suggests defining the characterization of bond considering the electron energy densities of kinetic, G_{BCP} , the potential, V_{BCP} and the total, H_{BCP} at BCP together with $\nabla^2 \rho_{BCP}$. For closed-shell interaction, the kinetic energy dominates as $G_{BCP} > |V_{BCP}|$ and H_{BCP} are positive, whereas, for shared-shell interaction, H_{BCP} is negative, and the potential energy dominates $G_{BCP} < |V_{BCP}|$. Another criterion based on Espinosa [48] uses the ratio of $|V_{BCP}|/G_{BCP}$ to distinguish the region of covalent and non-covalent bonds. For shared shell interaction, $|V_{BCP}|/G_{BCP} > 2$ and closed-shell interaction, $|V_{BCP}|/G_{BCP} < 1$ whereas for intermediate type, $1 < |V_{BCP}|/G_{BCP} < 2$ as partially covalent nature. Thus a positive $\nabla^2 \rho_{BCP}$ with a negative value of H_{BCP} is obtained for coordinated or ionic bonds [49]. The second approximation for the intermolecular hydrogen bonds (HBs), which was proposed by Espinosa et al., is based on the correlation between the topology parameters of the potential electron density at the critical bond point, V_{BCP} , and a given HB within its corresponding energy of E_{HB} , given as the following empirical relation:

$$E_{HB} = \frac{1}{2} V_{BCP} \quad (11)$$

Thus, we have examined the all-topology parameters for the complexes as shown in Fig. 4. The values of ρ_{BCP}

with $\nabla^2\rho_{BCP}$, G_{BCP} , V_{BCP} , H_{BCP} , the ratio of $|V_{BCP}|/G_{BCP}$ are given in Table 3 for the selected complexes of BMSF-BENZ(O_{42})/AIP and BMSF-BENZ(N_{58})/ZnO correspond to those illustrated in Figs.4(a) and (b), respectively.

In the case of BMSF-BENZ(O_{42})/AIP given in Table 3, the kinetic energy dominates, $|V_{BCP}| < G_{BCP}$, $\nabla^2\rho(r)$ values, and H_{BCP} are positive at all BCPs. $\nabla^2\rho(r)$ has a significant positive value for the O_{42} - Al_{61} bond with a positive value of H_{BCP} and the ratio of $|V_{BCP}|/G_{BCP} < 1$, indicating ionic bond. Based on all the topology parameters of BMSF-BENZ(O_{42})/AIP derived from the electron density, a sign of $\nabla^2\rho(r)$, a sign of H, the ratio $|V|/G$, the bonds have non-covalent character as displayed in Table 3 that the ratio $|V_{BCP}|/G_{BCP}$ of all interactions for BMSF-BENZ(O_{42})/AIP complex smaller than 1 implies that interaction between BMSF-BENZ(O_{42}) and AIP nanocage is composed of weak interactions including van der Waals type and intermolecular bonds. We have calculated hydrogen bond energy for O_{42} - Al_{61} using the criterion in Eq. 11. E_{HB} energy is obtained as (-29.57) kcal/mol for O_{42} - Al_{61} because it is due to the bonds of H_{33} - O_{42} - Al_{61} , which can be observed in Fig. 4. Thus, the E_{HB} energy value more significant than -10 kcal/mol points to the presence of hydrogen bonding and intermolecular solid bonds.

In the case of BMSF-BENZ(N_{58})/ZnO given in Table 3, interactions corresponding to the bonds of N_{58} - Zn_{65} and H_{57} - O_{68} , are partially covalent character with the topology

parameters of $\nabla^2\rho(r) > 0$ and $H_{BCP} < 0$ and the ratio of $1 < |V_{BCP}|/G_{BCP} < 2$. The E_{HB} energies for those intermolecular bonds are calculated as (-32.43 kcal/mol) and (-5.91 kcal/mol) for N_{58} - Zn_{65} and H_{57} - O_{68} , respectively. The E_{HB} value of (-32 kcal/mol) indicates the strong interaction and H-bond. It is a C-N-Zn type bond that was reported earlier.

However, other interactions between drug (N_{58}) and ZnO can be classified as a non-covalent character with the topology parameters of $\nabla^2\rho(r) > 0$ and $H_{BCP} > 0$, and the ratio of $|V_{BCP}|/G_{BCP} < 1$. It is evident in Fig. 4(b) that the bonds are between C_{59} - Zn_{65} , H_{62} - O_{66} and H_{61} - O_{67} atoms with van der Waals and O-H...H type interactions, respectively.

2.3. NCI/ RDG Analysis

Despite these theoretical insights, it is not clear to identify the interaction as a non-covalent bond. Therefore, the NCI analysis is the second powerful way based on the averaged reduced density gradient (RDG) method to analyze the type of the non-covalent interaction. It can be regarded as an extension of the QTAIM theory for visual study. The RDG function is defined as:

$$RDGs = \frac{1}{2(3\pi^2)^{1/3}} \frac{|\Delta\rho(r)|}{\rho(r)^{4/3}} \quad (12)$$

Table 3.

QTAIM parameters of selected complexes at the BCPs.

Struc.	BCPs Drug/ncage	ρ_{BCP}	$\nabla^2\rho_{BCP}$	G_{BCP}	V_{BCP}	H_{BCP}	$ V_{BCP} /G_{BCP}$
O_{42}/AIP	O_{42} - Al_{61}	0.060	0.450	0.103	-0.093	0.009	0.908
	H_7 - P_{62}	0.005	0.018	0.003	-0.002	0.001	0.683
	C_{49} - Al_{65}	0.002	0.004	0.001	$-0.82 \cdot 10^{-3}$	$0.21 \cdot 10^3$	0.796
N_{58}/ZnO	N_{58} - Zn_{65}	0.069	0.228	0.080	-0.102	-0.022	1.286
	C_{59} - Zn_{65}	0.009	0.043	0.007	-0.005	0.002	0.634
	H_{57} - O_{68}	0.022	0.070	0.018	-0.018	$-0.551 \cdot 10^{-3}$	1.030
	H_{62} - O_{66}	0.013	0.044	0.010	-0.010	$0.403 \cdot 10^{-3}$	0.962
	H_{61} - O_{67}	0.011	0.039	0.009	-0.008	$0.655 \cdot 10^{-3}$	0.928

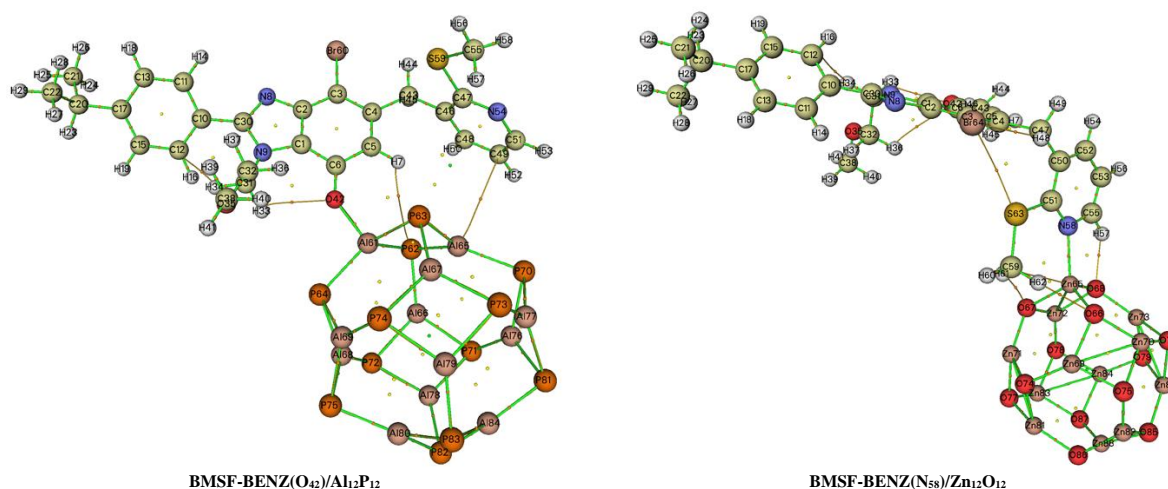


Fig. 4. The molecular topographical map of $O_{42}/Al_{12}P_{12}$ and $N_{58}/Zn_{12}O_{12}$ structures with all decisive points. The atomic and bond critical points are exhibited by atom labels and orange balls, respectively. The cages and ring critical points are proper to green and yellow circles, and the lines are bond paths.

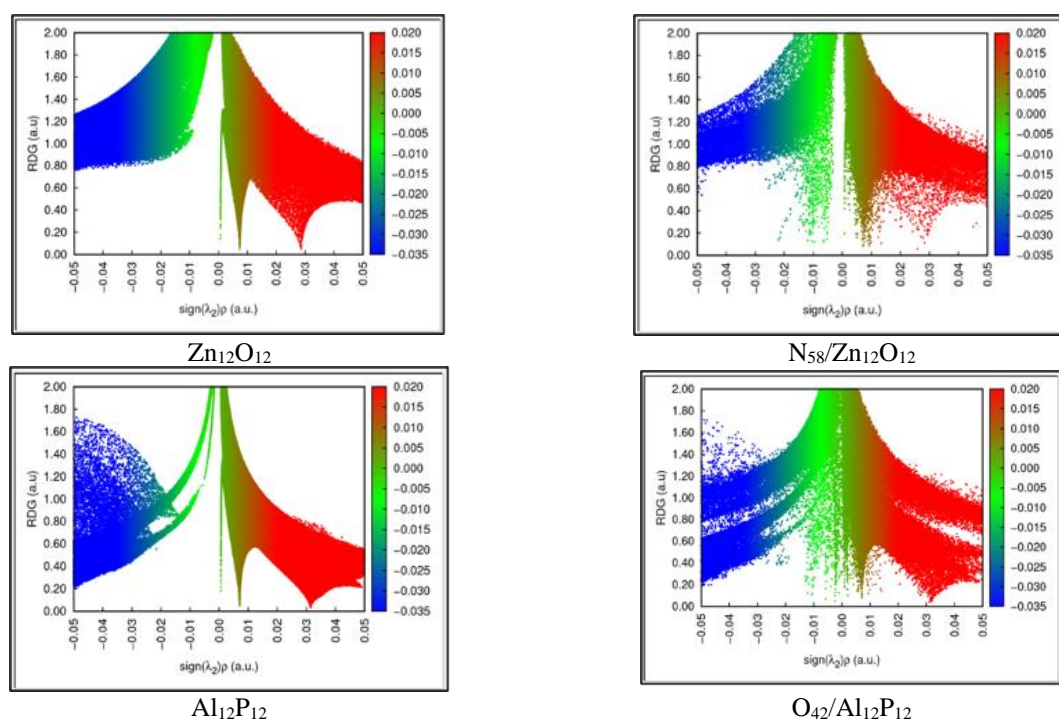


Fig. 5. Colour filled RDG scatter plots for $\text{Al}_{12}\text{P}_{12}$ nanocage, $\text{O}_{42}/\text{Al}_{12}\text{P}_{12}$ complex, $\text{Zn}_{12}\text{O}_{12}$ nanocage and $\text{N}_{58}/\text{Zn}_{12}\text{O}_{12}$ complex structure. Blue regions due to the strong, attractive interactions, green regions to the van der Waals interaction, and red regions to the strong repulsive interactions with steric effect.

RDG analysis can find non-covalent interactions determined through the $\text{sign } \lambda_2$, the second-largest eigenvalue of the Hessian matrix of $\rho(r)$. NCI analysis is generated at 0.5 au isosurface value by plotting RDG versus $(\text{sign } \lambda_2) \rho(r)$ as illustrated in Fig. 5 (a-d). NCI plots are created to investigate the existence of weak interactions. In the NCI/RDG analysis, the exchanges can be classified into three types due to the sign $(\text{sign } \lambda_2) \rho(r)$. If the $(\text{sign } \lambda_2) \rho < 0$, interactions are a strong attraction, the weak van der Waals interaction corresponds to $(\text{sign } \lambda_2) \rho \approx 0$, and if $(\text{sign } \lambda_2) \rho > 0$ the solid repulsive interactions (steric effect in ring cage) can be defined. The regions of the RDG scatter plots (as shown in a horizontal line in Fig. 5) can be classified into the value of $(\text{sign } \lambda_2) \rho$ as the red, green, and blue color codes. The color-filled RDG plots represent the types of interaction according to the color codes (details are given in Fig. 5.) The blue regions are solid and attractive interactions, and green regions indicate van der Waals interactions, and red regions represent repulsion interactions.

We have obtained the values of $(\text{sign } \lambda_2) \rho$ using NCI-RDG analysis by MULTIWFN. We have discussed RDG scatter plots given in Fig.5 using the values of $(\text{sign } \lambda_2) \rho$ together with the topology parameters of QTAIM analysis given in Table 3. The visual graphs of the NCI iso surfaces correspond to the interactions between nanocages and BMSF-BENZ drug given in Fig.6. Those graphs have created by VMD program based on the RDG scatter points in Fig. 5.

According to the coloured RDG scatter plots given in Fig 5, we define the range of colour codes. The larger negative values of $(\text{sign } \lambda_2) \rho$ ranging from -0.015 to -0.05 au are used to describe stabilizing hydrogen bond,

van der Waals types interactions are ranging in -0.015 to 0.01au, the destabilizing steric interactions correspond to the 0.01-0.05 au range.

It noticeable from Figs. 5, that there are van der Waals 6b between $\text{H}_{61}-\text{Zn}_{65}$ atoms as unreported topology parameters in Table 3. interaction region about $\rho = 0$ in pristine $\text{Al}_{12}\text{P}_{12}$ and $\text{Zn}_{12}\text{O}_{12}$ nanocages, respectively. Similarly, the van der Waals effect as the green region can be observed in $\text{O}_{42}/\text{Al}_{12}\text{P}_{12}$ and $\text{N}_{58}/\text{Zn}_{12}\text{O}_{12}$. The number of RDG points for the $\text{O}_{42}/\text{Al}_{12}\text{P}_{12}$ complex (see Fig. 5) increases more than $\text{N}_{58}/\text{Zn}_{12}\text{O}_{12}$ compared with those of the pristine ones in the van der Waals region. Thus, more non-covalent interactions for the $\text{O}_{42}/\text{Al}_{12}\text{P}_{12}$ complex are evident than that of $\text{N}_{58}/\text{Zn}_{12}\text{O}_{12}$.

For $\text{N}_{58}/\text{Zn}_{12}\text{O}_{12}$ complex, there are evident slight spikes in a range of -0.02au and -0.03au (indicated by blue color), which demonstrate robust and attractive interaction. Despite $\text{N}_{58}/\text{Zn}_{12}\text{O}_{12}$ complex, there is a small number of RDG points around -0.02au (see Fig.5), there is no noticeable spike in the vital interaction region for $\text{O}_{42}/\text{Al}_{12}\text{P}_{12}$ complex.

In Fig. 6, the NCI iso-surfaces with green or green-brown colour circles indicate van der Waals interactions, blue and red circles due to the strong attraction and repulsive interactions, respectively. The weak vdW type interaction can be determined by the greenish-brown circle.

For the $\text{O}_{42}/\text{Al}_{12}\text{P}_{12}$ complex given in Fig. 6(a), the value of $(\text{sign } \lambda_2) \rho$ for the interaction of $\text{O}_{42}-\text{Al}_{61}$ is about -0,060 au; there is too strong attraction placed in the blue colour region, but out of range of RDG scatter plots of Fig. 5(b). However, the dark blue circle can be observed on the region between Al and O atoms corresponding to that interaction at the left-hand side of Fig 6a. The

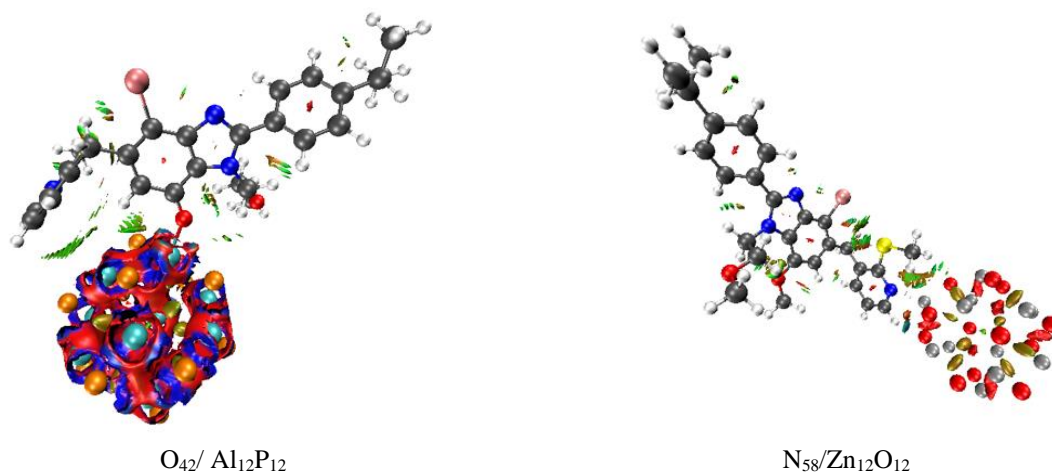


Fig. 6. The NCI iso-surface plots for $O_{42}/Al_{12}P_{12}$ and $N_{58}/Zn_{12}O_{12}$ complex structures where C, H, O, N, Al, P and Zn atoms are shown in grey, white, red, blue, cyan, orange and silver, respectively.

$(sign\lambda^2)\rho$'s value for the interactions between H7-P62 and C49-Al65 atoms are $-0.0058a.u$ and $-0.0024a.u$, respectively. Those interactions are vdW type characters illustrated by green circles between the corresponding atoms in Fig. 6a and confirm the QTAIM analysis in Table 3. On the other hand, blue and red circles can be observed inside the AIP nanocage in Fig. 6a, indicating the strong attractive and repulsive interactions due to the blue and red region scatter points given in Fig. 5b. It can be noticed in Fig. 6a that there are some greenish-brown circles inside the AIP nanocage due to the mixed van der Waals type interactions corresponding to the range $0.0 - 0.01a.u$ in Fig. 5b.

In the case of $N_{58}/Zn_{12}O_{12}$ complex, the value of $(sign\lambda^2)\rho$ is $-0.069a.u$. due to the strong attraction between N58 and Zn65 atoms indicated as partially covalent bond by QTAIM analysis given in Table 3 while it was illustrated as dark blue small circles in Fig. 6. For the interaction of C59-Zn65 atoms, the weak van der Waals interaction placed in plots of $N_{58}/Zn_{12}O_{12}$ complex in Fig. 6 with green circle. The partially covalent bond of H57-O68 is due to the dark blue circle between corresponding atoms shown in Fig. 6. Almost other interaction regions in green for H62-O66 and H61-O67 bonds can be observed in the NCI isosurface graphs of Fig. 6. Furthermore, greenish-brownish isosurface colour indicates slightly stronger vdW interactions, as is evident from Fig. 6 between H61-Zn65 atoms as unreported topology parameters in Table 3.

NCI-RDG analysis demonstrates that interactions between the drug and the ZnO nanocage surface are more substantial than AIP nanocage, which is compatible with the QTAIM results given in Table 3 and the adsorption energy values given in Table 2. Our results agree with a recent study, which reported that ZnO nanocages could be used as an intelligent nano-drug delivery system for ZnO/quercetin composite based on its RDG-NCI analysis [50].

2.4. The Electronic properties and the relative stability

Before adsorption, HOMO and LUMO Energies of ZnO nanocage were $(-6.99$ and $-2.86)$ eV with a Fermi

level of (-4.92) eV. The bandgap in ZnO is (4.12) eV. The HOMO in ZnO nanocage is mainly located on Oxygen atoms, while the LUMO has a uniform density on Zinc atoms. After interaction with BMSF-BENZ, notable changes are observed in HOMO and LUMO. In the BMSF-BENZ/ZnO complexes, the HOMO is further localized at nitrogen atoms on the drug compound (benzene ring), whereas the density in LUMO is localized at the atoms of the nanocage. During the interaction with BMSF-BENZ, energies of HOMO and LUMO were increased to $(-6.02, -5.99, -5.73, -5.69, -5.74, -5.95, -5.89)$ eV and $(-2.10, -2.00, -2.26, -2.40, -2.31, -1.91, -2.11)$ eV respectively for the active atoms of the drug compound, whereas the bandgap is decreased $(3.92, 3.98, 3.46, 3.28, 3.43, 4.04, 3.78)$ eV.

Again, A drop in the bandgap $(3.22, 3.11, 3.22, 2.84, 2.88, 2.74, 3.20)$ eV was also recognized for adsorption of BMSF-BENZ on AIP nanocage. However, a slight difference is observed in interaction with BMSF-BENZ. The HOMO in the AIP-BMSF-BENZ complex is located on drug atoms close to the binding site, whereas the LUMO is located on Al and P atoms away from the binding site (see Fig. 6 for details). The frontier molecular orbitals are given in Fig. 6.

For better understanding the mechanism of sensing of the nanocages to the drug, the percentage variation of $\% \Delta E_g$ energy gap during the adsorption process is calculated by the following equation:

$$\% \Delta E_g = 100 \times (E_{g2} - E_{g1}) / E_{g1} \quad (13)$$

Where E_{g2} and E_{g1} are the E_g values of the complexes structures and the nanocage, respectively, the change values percentage of $\% \Delta E_g$ for each structure are given in Table 4. The density of states (DOS) of pure nano- and BMSF-BENZ nano-adsorbents were also studied in order to understand the interaction of BMSF-BENZ with these nano-adsorbents. The density of the nanocage state in its pure geometry was compared with that of the new complexes generated after the adsorption process with the BMSF-BENZ complex (see Fig. 7). When interacting with BMSF-BENZ, some new energy states appear near the

Table 4

E_{HOMO} , E_{LUMO} , Fermi level energies (E_f) in (eV), Energy gap (E_g), The dipole moment (DM) in Depye of the pure nanocages and the new complexes

System	E_{HOMO}	E_{LUMO}	E_g	ΔE_g	E_f	DM	System	E_{HOMO}	E_{LUMO}	E_g	ΔE_g	E_f	DM
Zn ₁₂ O ₁₂	-6.99	-2.86	4.12	-	-4.92	1.06	Al ₁₂ P ₁₂	-6.74	-3.36	3.37	-	-5.05	0
Br	-6.02	-2.10	3.92	-4.85	-4.06	15.06	Br	-6.07	-2.85	3.22	-4.45	-4.46	20.42
N ₈	-5.99	-2.00	3.98	-3.39	-4.00	18.09	N ₈	-5.66	-2.54	3.11	-7.71	-4.10	44.95
N ₉	-5.73	-2.26	3.46	-16.02	-4.00	8.42	N ₉	-6.09	-2.86	3.22	-4.45	-4.47	5.73
N ₅₈	-5.69	-2.40	3.28	-20.39	-4.04	7.37	N ₅₈	-5.75	-2.90	2.84	-15.73	-4.33	8.04
O ₃₅	-5.74	-2.31	3.43	-16.75	-4.03	3.32	O ₃₅	-5.86	-2.97	2.88	-14.54	-4.41	7.48
O ₄₂	-5.95	-1.91	4.04	-1,94	-3.93	5.10	O ₄₂	-5.74	-3.00	2.74	-18.69	-4.37	1.77
S	-5.89	-2.11	3.78	-8.25	-4.00	7.68	S	-5.80	-2.60	3.20	-5.04	-4.20	22.46

Fermi level of all complexes, which leads to lower E_g values. The most significant change in E_g was observed for the BMSF-BENZ(N₅₈)/ZnO complex ($E_g = 3.28$), followed by the BMSF-BENZ(O₄₂)/AIP complex ($E_g = 2.74$). The change in E_g for a BMSF-BENZ (N₅₈)/ZnO complex is expected to cause significant changes in electrical conductivity because it is a significant factor in determining the electrical conductivity of a material and the difference between E_g between a new complex and a nanocage is 0.84 eV.

Dipole moment indicates the polarity of the compound where it appears due to the asymmetric charge distribution as well as the difference in electronegativity between the resultant molecules or atoms, where the large dipole moment refers to the more polar structure, which results in a more stable interaction of the system [51].

The dipole moment results showed that the new compounds obtained from the adsorption of the BMSF-BENZ compound on the surface of the nanocage had different values more significant than the drug's value before adsorption. A more stable reaction occurred when the drug compound was adsorbed on the surface of the AIP nanocage at N₈ atom with the value of (44.95) Debye, which was more significant than the rest of the other active atoms of the drug compound.

2.5. Quantum molecular descriptors

The universal reactivity criteria are major parameters because they represent a molecule's reactivity and stability or complexity. BMSF-BENZ is harder (2.26 eV) compared to nanocages investigated. It was noticeable, the hardness for the nanocages decreased on the new complexes. For ZnO nanocage, the hardness is ($\eta = -0.30, -0.26, -0.53, -0.61, -0.54, -4.28, -0.37\text{eV}$) for all active atoms in the drug molecule (Br, N₈, N₉, N₅₈, O₃₅, O₄₂, and S) respectively. While significantly substantial changes are observed for AIP nanocage ($\eta = -0.57$) and for the active atoms of the drug ($\eta = -0.65, -0.70, -0.65, -0.84, -0.81, -0.89, -0.66\text{ eV}$). Hardness measures the stability of the chemical system across deformation in the presence of an electrical field; the BMSF-BENZ/nanocage complexes are more predisposed to changes under electrical fields

than pure nanocages. Consequently, it is expected that softness for the new complexes will increase. Values of softness on adsorption of BMSF-BENZ the nanocages are given in Table 5.

The potential chemical increased for all nanocages on the new complexes. For ZnO, chemical potential increased from (-4.92) eV to (-4.06, -4.00, -4.00, -4.04, -4.03, -3.93, -4.00) eV respectively for all active atoms in drug molecule. Furthermore, the chemical potentials of AIP nanocage increased from (-5.05) eV. The greatest change in chemical potential was noticed for ZnO at O₄₂ atom, and AIP was at atom N₈. An approximately different trend was observed for electrophilicity. For ZnO nanocage, electrophilicity decreases, but on AIP nanocage, there was a noticeable increase except in the N₈ atom (Table 5).

The positive values of ΔH and G intimate that the reaction process is endothermic instead of spontaneous. On the other hand, negative values of ΔH and G indicate that the reaction is an exothermic and spontaneous process [52] (see Table 6).

The calculated data of ΔH and ΔG were negative values in all the new complexes, which are dynamically stable. Also, the most negative value of ΔS indicates the most ordered compound. So, the calculated thermodynamic parameters prophesy that the investigated complexes are more suitable and thermodynamically enduring for BMSF-BENZ drug delivery.

As a method to ensure structural stability, and by using a specific infrared (IR) spectroscopy on the studied BMSF-BENZ/nanocage complexes, the results of the frequencies of the new complexes showed that the frequency range had changed from 3245.15 cm^{-1} in the case of BMSF-BENZ to varying values ranging between 3227.90 cm^{-1} as a value for BMSF-BENZ(N₅₈)/ZnO and 3235.05 cm^{-1} as a value for BMSF-BENZ(N₅₈)/AIP (Table 6), which proves that the intensity of the frequencies has changed to values near to the average. Therefore these values indicate an excellent interaction intensity between the nanocages and the drug compound, especially when the interaction

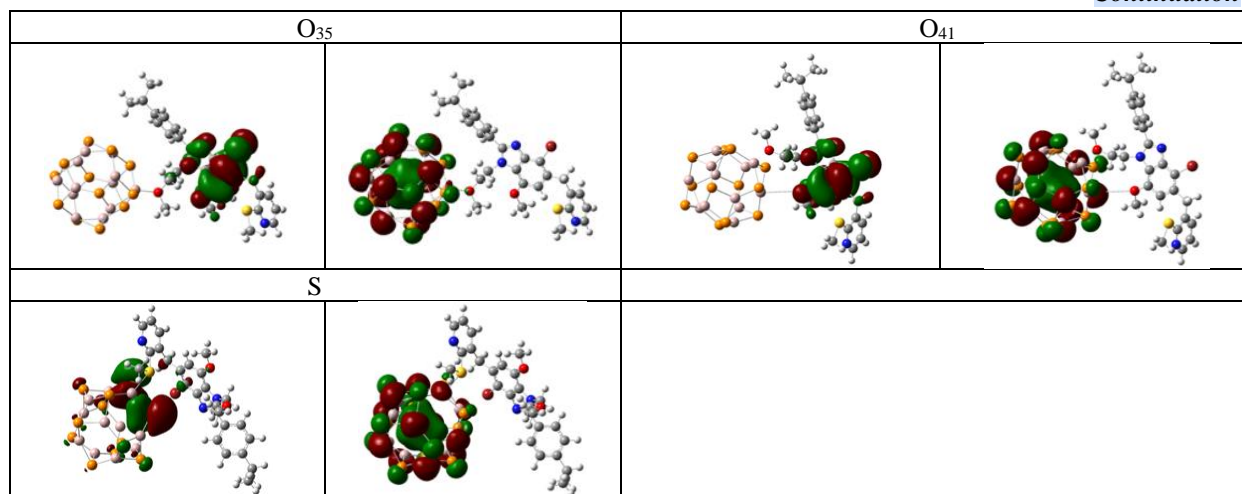


Fig. 7. The optimized structure, HOMO-LUMO distributions of pure nanocages along with the new complex with BMSF-BENZ.

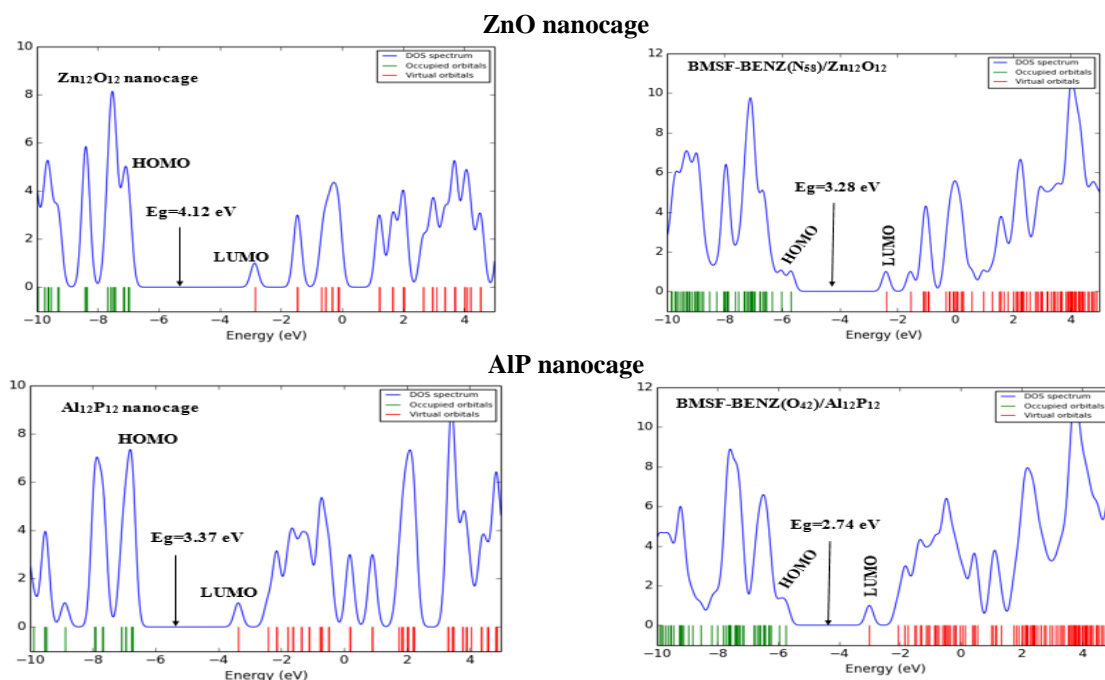


Fig. 8. TDOS graphs for pristine $Zn_{12}O_{12}$, and $Al_{12}P_{12}$ nanocage and BMSF-BENZ- $O_{42}/Al_{12}P_{12}$, BMSF-BENZ- $N_{58}/Zn_{12}O_{12}$ complexes structures

Table 5

Chemical potential (μ), hardness (η), softness (S), and electrophilicity (ω) of the optimized structure of BMSF-BENZ adsorbed on ZnO, and AlP nanocages

Structure	Chemical potential (μ)	Hardness (η)	Softness (S)	Electrophilicity (ω)	Structure	Chemical potential (μ)	Hardness (η)	Softness (S)	Electrophilicity (ω)
Drug	-3.14	2.26	0.44	2.18					
$Zn_{12}O_{12}$	-4.92	2.06	0.48	5.87	$Al_{12}P_{12}$	-5.05	1.68	0.59	7.56
Br	-4.06	1.96	0.50	4.20	Br	-4.46	1.61	0.62	6.19
N_8	-4.00	1.99	0.50	4.01	N_8	-4.10	1.55	0.64	5.41
N_9	-4.00	1.73	0.57	4.61	N_9	-4.47	1.61	0.61	6.21
N_{58}	-4.04	1.64	0.60	4.97	N_{58}	-4.33	1.42	0.70	6.59
O_{35}	-4.03	1.71	0.58	4.74	O_{35}	-4.41	1.44	0.69	6.75
O_{42}	-3.93	2.02	0.49	3.82	O_{42}	-4.37	1.37	0.72	6.98
S	-4.00	1.89	0.52	4.24	S	-4.20	1.60	0.62	5.51

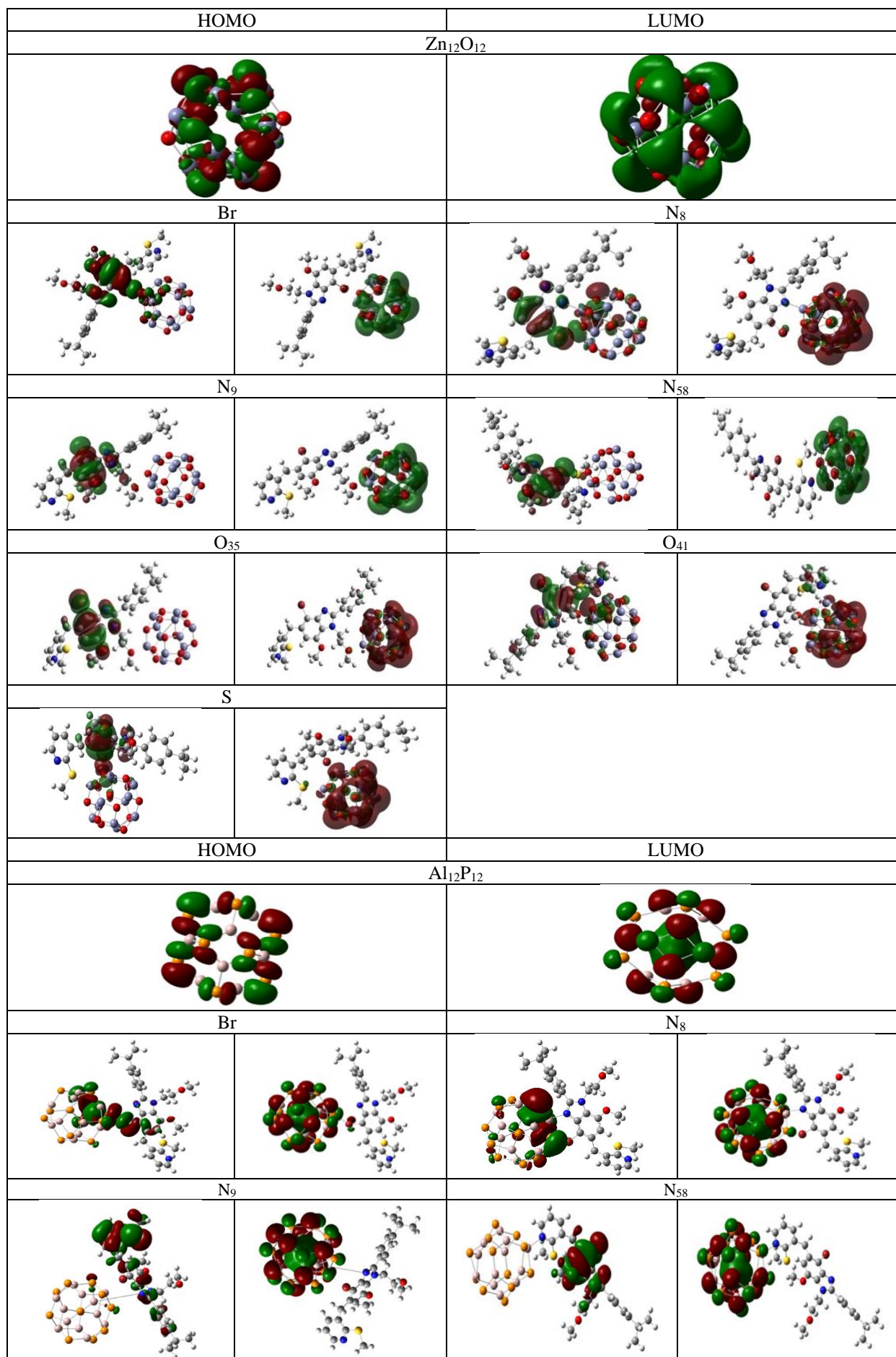


Table 6

The new complexes Gibbs free energy(ΔG) in kcal.mol⁻¹, The change of enthalpy(ΔH) in kcal.mol⁻¹, The change of entropy(ΔS) in kcal/mol.K, and the minimum and maximum frequency in cm⁻¹

Structure	ΔG	ΔH	ΔS	V_{\min}	V_{\max}	Structure	ΔG	ΔH	ΔS	V_{\min}	V_{\max}
Zn ₁₂ O ₁₂						Al ₁₂ P ₁₂					
Br	-21.55	-31.91	-0.03	4.56	3237.39	Br	-10.81	-21.34	-0.03	1.70	3248.99
N ₈	-33.62	-47.99	-0.04	8.32	3248.04	N ₈	-30.35	-45.78	-0.05	7.20	3249.07
N ₉	-23.76	-36.02	-0.04	6.01	3242.64	N ₉	-7.91	-21.21	-0.04	5.59	3248.49
N ₅₈	-20.94	-34.62	-0.04	5.16	3227.90	N ₅₈	-19.23	-30.99	-0.03	4.51	3241.98
O ₃₅	-23.54	-37.82	-0.04	7.35	3245.70	O ₃₅	-18.71	-29.98	-0.03	5.06	3243.66
O ₄₂	-47.71	-65.79	-0.06	10.65	3231.67	O ₄₂	-18.55	-29.61	-0.03	3.45	3244.44
S	-28.66	-42.11	-0.04	4.40	3247.90	S	-14.47	-27.89	-0.04	5.88	3235.05

between the drug compound and (BMSF-BENZ(N₈)/AIP) was at the nitrogen atom [53]. On the other hand, the positive values of the vibrations indicate that the reaction is stable with minimal waste energy [54].

Conclusions

In summary, the B3LYP/6-31G(d,p) calculations method was employed to investigate the adsorption interaction of BMSF-BENZ drug on the surfaces of Zn₁₂O₁₂ and Al₁₂P₁₂ nanocages in the gas phase. After complete structural relaxation of the stable configurations, the binding energy, the bond distance, and the necessary physical parameters were investigated. The essential interaction energy of BMSF-BENZ was obtained for Zn₁₂O₁₂, and Al₁₂P₁₂ nanocages on all active atoms in the BMSF-BENZ molecule (seven different locations). Charge analyses and the plots of the molecular electrostatic potential revealed that the electronic

properties of all nanocages were significantly affected by the adsorption of BMSF-BENZ. Furthermore, the density of states and HOMO-LUMO distributions revealed extraordinary orbital hybridization between BMSF-BENZ and the investigated nanocages.

In conclusion, all the nanostructures under investigation are promising nominees for sensing BMSF-BENZ molecules, while Zn₁₂O₁₂ nanocage can be considered a drug delivery carrier for BMSF-BENZ drug.

Zaid H. Al-Sawaff – Ph.D., (Medical instrumentation technology), lecturer;

Serap Senturk Dalgic – Ph.D. (Physics) Prof., lecturer;

Zaheda A. Najim – Ph.D., (Physical chemistry), Assist. Prof, lecturer;

Shatha S. Othman – Ph.D., (physical chemistry), Assist Prof, lecturer;

Fatma Kandemirli – Ph.D., (chemical engineering) Prof., Head of biomedical engineering dept.

- [1] J.A. Kanis, C. Cooper, R. Rizzoli, & J.Y. Reginster, *Osteoporosis International* 30(1), 3 (2019); <https://doi.org/10.1007/s00198-018-4704-5>; 31(1), 209 (2020); <https://doi.org/10.1007/s00198-019-05184-3>.
- [2] S.P. Tuck, R.M. Francis, *Osteoporosis. Postgraduate Medical Journal* 78(923), 526 (2002); <https://doi.org/10.1136/pmj.78.923.526>.
- [3] C. Deal, *Nature Clinical Practice Rheumatology* 5(1), 20 (2009); <https://doi.org/10.1038/ncprheum0977>.
- [4] Ahmed Hassen Shntaif, Z.M. Rashid, Z.H., Al-Sawaff, & F. Kandemirli, *Russian Journal of Bioorganic Chemistry* 47(3), 777 (2021); <https://doi.org/10.1134/S106816202103016X>.
- [5] P.D. Dwivedi, A. Tripathi, K.M. Ansari, R. Shanker, & M. Das, *Journal of Biomedical Nanotechnology*, 7(1), 193 (2011); <https://doi.org/10.1166/jbn.2011.1264>.
- [6] X. Lv, P. Wang, R. Bai, Y. Cong, S. Suo, X. Ren, & C. Chen, *Biomaterials* 35(13), 4195 (2014); <https://doi.org/10.1016/j.biomaterials.2014.01.054>.
- [7] Q. Yu, J. Li, Y. Zhang, Y. Wang, L. Liu, & M. Li, *Scientific Reports* 6 (May), 26667 (2016); <https://doi.org/10.1038/srep26667>.
- [8] A.F. Halbus, T.S. Horozov, & V.N. Paunov, *ACS Applied Materials and Interfaces* 11(42), 38519 (2019); <https://doi.org/10.1021/acsami.9b14403>.
- [9] S. Hussain, R. Hussain, M.Y. Mehboob, S.A.S. Chatha, A.I. Hussain, A. Umar, ... K. Ayub, *ACS Omega* 5(13), 7641 (2020); <https://doi.org/10.1021/acsomega.0c00507>.
- [10] A.L. Silva, L.I.F. Moura, B. Carreira, J. Coniot, A.I. Matos, C. Peres, ... H.F. Florindo, *Functional Moieties for Intracellular Traffic of Nanomaterials. Biomedical Applications of Functionalized Nanomaterials: Concepts, Development and Clinical Translation*. Elsevier Inc. (2018); <https://doi.org/10.1016/B978-0-323-50878-0.00014-8>.
- [11] J.K. Patra, G. Das, L.F. Fraceto, E.V.R. Campos, M.D.P. Rodriguez-Torres, L.S. Acosta-Torres, H.S. Shin, *Journal of Nanobiotechnology* 16(1), 1 (2018); <https://doi.org/10.1186/s12951-018-0392-8>.
- [12] S.S. Suri, H. Fenniri, & B. Singh, *Journal of Occupational Medicine and Toxicology* 2(1), 1 (2007); <https://doi.org/10.1186/1745-6673-2-16>.

- [13] A.P. Singh, A. Biswas, A. Shukla, & P. Maiti, *Signal Transduction and Targeted Therapy* 4(1), 1 (2019); <https://doi.org/10.1038/s41392-019-0068-3>.
- [14] D. Scarano, F. Cesano, S. Bertarione, & A. Zecchina, *Crystals* 8(4), (2018); <https://doi.org/10.3390/cryst8040153>.
- [15] K.S. Siddiqi, A. Tajuddin ur Rahman, & A. Husen, *Nanoscale Research Letters* 13, (2018); <https://doi.org/10.1186/s11671-018-2532-3>.
- [16] X. Zhang, W. Lan, J. Xu, Y. Luo, J. Pan, C. Liao, ... X. Huang, *Sensors and Actuators, B: Chemical* 289, 144 (2019); <https://doi.org/10.1016/j.snb.2019.03.090>.
- [17] M.T. Baei, M.B. Tabar, & S. Hashemian, *Adsorption Science and Technology* 31(5), 469 (2013); <https://doi.org/10.1260/0263-6174.31.5.469>.
- [18] S. Khan, M.A. Gilani, S. Munsif, S. Muhammad, R. Ludwig, & K. Ayub, *Journal of Molecular Graphics and Modelling* 106 (April), 107935 (2021); <https://doi.org/10.1016/j.jmgm.2021.107935>.
- [19] H.R. Ghenaatian, M.T. Baei, & S. Hashemian, *Superlattices and Microstructures* 58, 198 (2013); <https://doi.org/10.1016/j.spmi.2013.03.006>.
- [20] J. Beheshtian, Z. Bagheri, M. Kamfiroozi, & A. Ahmadi, *Journal of Molecular Modeling* 18(6), 2653 (2012); <https://doi.org/10.1007/s00894-011-1286-y>.
- [21] A. Shokuhi Rad, & K. Ayub, *Journal of Alloys and Compounds* 672, 161 (2016); <https://doi.org/10.1016/j.jallcom.2016.02.139>.
- [22] E.F. Archibong, R.M. Gregorius, & S.A. Alexander, *Chemical Physics Letters* 321(3-4), 253 (2000); [https://doi.org/10.1016/S0009-2614\(00\)00355-9](https://doi.org/10.1016/S0009-2614(00)00355-9).
- [23] A. Shokuhi Rad, S. Ghasemi Ateni, H.A., Tayebi, P. Valipour, & V. Puralijan Foukolaei, *Journal of Sulfur Chemistry* 37(6), 622 (2016); <https://doi.org/10.1080/17415993.2016.1170834>.
- [24] A.S. Rad, *Applied Surface Science* 357(2), 1217 (2015); <https://doi.org/10.1016/j.apsusc.2015.09.168>.
- [25] M.T. Baei, M. Koochi, & M. Shariati, *Journal of Molecular Structure* 1159, 118 (2018); <https://doi.org/10.1016/j.molstruc.2018.01.022>.
- [26] J. Lv, C. Zhang, S. Wang, M. Li, & W. Guo, *Analyst* 146(2), 605 (2021); <https://doi.org/10.1039/d0an01383h>.
- [27] H. Wu, X. Fan, & J.L. Kuo, *International Journal of Hydrogen Energy* 37(19), 14336 (2012); <https://doi.org/10.1016/j.ijhydene.2012.07.081>.
- [28] M. Pandurangan, & D.H. Kim, *Saudi Journal of Biological Sciences* 22(6), 679 (2015). <https://doi.org/10.1016/j.sjbs.2015.03.013>.
- [29] J. Zhang, H. Lu, L. Zhang, D. Leng, Y. Zhang, W. Wang, ... C. Wang, *Sensors and Actuators, B: Chemical*, 291(April), 458 (2019); <https://doi.org/10.1016/j.snb.2019.04.058>.
- [30] M.T. Baei, M.B. Tabar, & S. Hashemian, *Adsorption Science and Technology* 31(5), 469 (2013); <https://doi.org/10.1260/0263-6174.31.5.469>.
- [31] M. Ghorbanzadeh Ahangari, & A. Hamed Mashhadzadeh, *International Journal of Hydrogen Energy* 45(11), 6745 (2020); <https://doi.org/10.1016/j.ijhydene.2019.12.106>.
- [32] Z. Al-Sawaff, S. Dalgic Senturk, & F. Kandemirli, *European Journal of Chemistry* 12(3), 314 (2021); <https://doi.org/10.5155/eurjchem.12.3.314-322.2143>.
- [33] Merve Şengül ALPATER, Zaid H. AL-SAWAFF, & Fatma KANDEMİRLİ. (2021). Theoretical study of gallium nitride nanocage as a carrier for Cisplatin anticancer drug. *Global Journal of Engineering and Technology Advances*, 9(3), 077–085. <https://doi.org/10.30574/gjeta.2021.9.3.0166>.
- [34] R. Ahmadi, & M. Ebrahimikia, *Physical Chemistry Research* 5(4), 617 (2017); <https://doi.org/10.22036/pcr.2017.70859.1337>.
- [35] P. Lakshmi Praveen, & D.P. Ojha, *Phase Transitions* 87(5), 515 (2014); <https://doi.org/10.1080/01411594.2013.852195>.
- [36] A. Maleki, *Structural Chemistry* (0123456789), (2021); <https://doi.org/10.1007/s11224-021-01842-7>.
- [37] P.L. Praveen, & D.P. Ojha, *Journal of Molecular Liquids* 194, 8 (2014); <https://doi.org/10.1016/j.molliq.2014.01.002>.
- [38] P.L. Praveen, D.S. Ramakrishna, & D.P. Ojha, *Molecular Crystals and Liquid Crystals* 643(1), 76 (2017); <https://doi.org/10.1080/15421406.2016.1262702>.
- [39] P.L. Praveen, & D.P. Ojha, *Journal of Molecular Modeling* 18(4), 1513 (2012); <https://doi.org/10.1007/s00894-011-1171-8>.
- [40] H. Farrokhpour, H. Jouypazadeh, & S. Vakili Sohroforouzani, *Molecular Physics* 118(4), 1 (2020); <https://doi.org/10.1080/00268976.2019.1626506>.
- [41] R.F.W. Bader, *Atoms in molecules. Acc. Chem. Res* 18, 9 (1985); <https://doi.org/10.1021/ar00109a003>.
- [42] T. Lu, & F. Chen, *Journal of Computational Chemistry* 33(5), 580 (2012); <https://doi.org/10.1002/jcc.22885>.
- [43] W. Thomas, C. Kelley, 1 gnuplot (2004).
- [44] W. Humphrey, A. Dalke, K. Schulten, *J. Mol. Graph.* 14, 33 (1996).
- [45] Z. Al-sawaff, H. Sayiner, F. Kandemirli, Retrieved from (2020). <https://dergipark.org.tr/en/pub/jauist/issue/55760/739466>.
- [46] J. Beheshtian, Z. Bagheri, M. Kamfiroozi, & A. Ahmadi, *Journal of Molecular Modeling* 18(6), 2653 (2012); <https://doi.org/10.1007/s00894-011-1286-y>.
- [47] H.S. Sayiner, F. Kandemirli, S. Senturk Dalgic, M. Monajjemi, F. Mollaamin, *J. Mol. Model.* 28,11 (2022).

<https://doi.org/10.1007/s00894-021-04948-1>

- [48] D. Cremer and E. Kraka, *Angew. Chem., Int. Ed. Engl.* 23, 627 (1984).
 [49] E. Espinosa, I. Alkorta, J. Elguero and E. Molins, *J. Chem. Phys.* 117, 5529 (2002).
 [50] Abhishek Shahi and Elangannan Arunan, *Phys. Chem. Chem. Phys.* 16, 22935 (2014);
<https://doi.org/10.1039/c4cp02585g>.
 [51] P. Sathishkumar, Z. Li, R. Govindan et al, *Appl. Surf. Sci.* 536, 147741 (2021);
<https://doi.org/10.1016/j.apsusc.2020.147741>.
 [52] A.S. Rad, P. Valipour, A. Gholizade, & S.E. Mousavinezhad, *Chemical Physics Letters* 639, 29 (2015);
<https://doi.org/10.1016/j.cplett.2015.08.062>.
 [53] L. Chen, W. Feng, J. Fan, K. Zhang, & Z. Gu, *Science of the Total Environment* 711, 135155 (2020);
<https://doi.org/10.1016/j.scitotenv.2019.135155>.
 [54] A.S. Rad, & K. Ayub, *Journal of Alloys and Compounds* 678, 317 (2016);
<https://doi.org/10.1016/j.jallcom.2016.03.175>.

З. Х. Аль-Савафф^{1,2}, С. С. Далгік³, З.А. Нейджім⁴, Ш. С. Осман⁵, Ф. Кандермірлі⁶

Дослідження BMSF-BENZ хемосорбції на наноклітин Zn₁₂O₁₂, Al₁₂P₁₂ методами порівняльної теорії функціональної густини

¹Кафедра матеріалознавства та інженерії, факультет інженерії та архітектури, Університет Кастамону, Туреччина, zaidalsawaff@ntu.edu.iq

²Технологія медичних приладів, Технічний інженерний коледж, Північний технічний університет, Мосул, Ірак

³Кафедра фізики, факультет природничих наук, Тракійський університет, 22030, Едірне, Туреччина

⁴Освітній коледж чистої науки, Університет Мосула, Мосул, Ірак

⁵Технологія медичних приладів, Технічний інженерний коледж, Північний технічний університет, Мосул, Ірак

⁶Кафедра біомедичної інженерії, факультет інженерії та архітектури, Університет Кастамону, Кастамону, Туреччина

Досліджено потенціал і можливості наноклітин оксиду цинку та фосфіду алюмінію виявляти й адсорбувати молекулярний ((4-бром-7-метокси-1-(2-метоксиетил)-5-[[3-(метилсульфоніл) феніл]метил]-2-[4-(пропан-2-))іл]феніл]-1Н-1,3-бензотіазол). Для цього вибрано сім стабільних варіантів для адсорбції BMSF-BENZ на поверхні цих наноклітин. Усі розглянуті конфігурації оптимізовано з використанням теорії DFT на базовому наборі 6-31G** та V3LYP теорії. Далі, на основі оптимізованих структур застосовано квантову теорію атома в молекулі (QTAIM), аналіз градієнта пониженої густини (RDG) та молекулярно-орбітальний аналіз (МО).

Результати показали, що реакція BMSF-BENZ із наноклітинами була високоекзотермічною, що вказує на високу хімічну адсорбцію нових комплексів. Для всіх досліджених активних атомів у складі лікарського комплексу, енергія адсорбції на нанокаркасі ZnO була вищою, ніж у AlP, де енергії адсорбції становили (-28,20, -37,86, -27,36, -23,59, -30,30, -42,55 і - 32,49) Ккал/моль і (-17,03, -28,30, -15,45, -16,70, -18,22, -18,35 і -18,64) Ккал/моль для наноклітин ZnO та Al-P, відповідно.

Аналіз топології, зокрема, QTAIM та NCI/RDG, вказує на те, що взаємодії між препаратом BMSF-BENZ та поверхнею наноклітини ZnO є більш істотною, ніж взаємодія наноклітини AlP. Результати отриманого заряду, сумарної густини станів (TDOS) та молекулярно-орбітально-граничного аналізу підтверджують характерну орбітальну гібридизацію при адсорбції BMSF-BENZ, що свідчить про потенційне застосування AlP як біохімічного адсорбенту BMSF-BENZ. Тим не менш, наноклітини ZnO можуть бути кандидатами для застосування препаратів.

Ключові слова: адсорбція ліків; BMSF-BENZ; наноклітини; система доставки ліків; теорія функціоналу густини; термодинамічні властивості.